A multitargeted probe-based strategy to identify signaling vulnerabilities in cancers

Received for publication, November 26, 2018, and in revised form, March 1, 2019 Published, Papers in Press, March 11, 2019, DOI 10.1074/jbc.RA118.006805

Suman Rao[‡§¶], **Guangyan Du**[§¶], **Marc Hafner**[‡1], **Kartik Subramanian**[‡], **Peter K. Sorger**[‡], **and Nathanael S. Gray**[§¶2]

From the [‡]*Laboratory of Systems Pharmacology and* [¶]*Department of Biological Chemistry and Molecular Pharmacology, Harvard Medical School, Boston, Massachusetts 02115 and* [§]*Department of Cancer Biology, Dana-Farber Cancer Institute, Boston, Massachusetts 02115*

Edited by Eric R. Fearon

Most cancer cells are dependent on a network of deregulated signaling pathways for survival and are insensitive, or rapidly evolve resistance, to selective inhibitors aimed at a single target. For these reasons, drugs that target more than one protein (polypharmacology) can be clinically advantageous. The discovery of useful polypharmacology remains serendipitous and is challenging to characterize and validate. In this study, we developed a non-genetic strategy for the identification of pathways that drive cancer cell proliferation and represent exploitable signaling vulnerabilities. Our approach is based on using a multitargeted kinase inhibitor, SM1-71, as a tool compound to identify combinations of targets whose simultaneous inhibition elicits a potent cytotoxic effect. As a proof of concept, we applied this approach to a KRAS-dependent non-small cell lung cancer (NSCLC) cell line, H23-KRAS^{G12C}. Using a combination of phenotypic screens, signaling analyses, and kinase inhibitors, we found that dual inhibition of MEK1/2 and insulin-like growth factor 1 receptor (IGF1R)/insulin receptor (INSR) is critical for blocking proliferation in cells. Our work supports the value of multitargeted tool compounds with well-validated polypharmacology and target space as tools to discover kinase dependences in cancer. We propose that the strategy described here is complementary to existing genetics-based approaches, generalizable to other systems, and enabling for future mechanistic and translational studies of polypharmacology in the context of signaling vulnerabilities in cancers.

Over the last two decades cancer treatment has been revolutionized by a targeted approach to therapy in which a selective agent is developed to hit a single, specific target. Prominent examples of targeted therapies include selective kinase inhibitors that target BCR-ABL in chronic myelogenous leukemia or mutant EGFR[3] and EML4-ALK in nonsmall cell lung cancer (NSCLC) (1). Unfortunately, in some tumor types, this approach is limited by the rapid emergence of drug resistance; in other cancers with multiple or conventionally undruggable driver mutations, targeted approaches can be hard to apply. Many tumors are genetically heterogeneous, harboring multiple genomic alterations in different combinations, which results in signaling plasticity and rapid evolvability. These properties of tumors have generated interest in developing drugs capable of simultaneously inhibiting multiple signaling pathways. Such inhibitors, often described as "polypharmacological agents" have long been utilized therapeutically in CNS diseases, infection, inflammatory diseases, and psychiatric disorders where selective inhibitors have failed (2, 3). Examples of approved polypharmacological drugs include acetyl salicylic acid, paracetamol, clozapine, etc., which act by binding and interacting with several proteins, thereby exerting pharmacological effects that cannot be ascribed to a single molecular target (2).

In the field of kinase inhibitors, many approved drugs were developed with a particular target in mind but are now known to be multitargeted. Their multitargeting properties are a consequence of their binding mode. Kinase inhibitors have been developed to bind in conserved ATP-binding pockets and therefore have cross-reactivity toward other kinases with shared structural features in their active sites. The multitargeted nature of most approved kinase inhibitors has now been confirmed and characterized through kinome-wide profiling

This work was supported by National Institutes of Health Grants P50 GM107618, U54-CA225088, and U54-HL127365 (to S. R., M. H., K. S., and P. K. S.); a Jonathan M. Goldstein and Kaia Miller Goldstein systems pharmacology fellowship (to S. R.); and a Linde Family gift (to G. D.). N. S. G. is a founder, science advisory board member (SAB), and equity holder in Gatekeeper, Syros, Petra, C4, B2S, and Soltego. The Gray lab receives or has received research funding from Novartis, Takeda, Astellas, Taiho, Janssen, Kinogen, Voronoi, Her2llc, Deerfield, and Sanofi. P. K. S. is a founder, SAB member, and equity holder in Merrimack Pharmaceutical and Glencoe Software; he is on the Board of Directors of Applied Biomath and the SAB of RareCyte Inc. In the last five years the Sorger lab has received research funding from Novartis and Merck. M. H. is currently an employee of Genentech, Inc. The content is solely the responsibility of the authors and does not necessarily represent the official views of the National Institutes of Health.

This article was selected as one of our Editors' Picks.

This article contains Figs. S1–S3, Tables S1 and S2, and File S1.

[1] Present address: Dept. of Bioinformatics and Computational Biology, Genentech, Inc., South San Francisco, CA 94080.

[2] To whom correspondence should be addressed. E-mail: Nathanael_Gray@dfci.harvard.edu.

[3] The abbreviations used are: EGFR, epidermal growth factor receptor; NSCLC, nonsmall cell lung cancer; IGF1R, insulin-like growth factor 1 receptor; INSR, insulin receptor; CNS, central nervous system; PDGFR, platelet-derived growth factor receptor; VEGFR, vascular endothelial growth factor receptor; PI3K, phosphatidylinositol 3-kinase; SM1-71-R, reversible analog of SM1-71; MAPK, mitogen-activated protein kinase; ERK, extracellular signal-regulated kinase; MEK, MAPK/ERK kinase; TNBC, triple-negative breast cancer; GR, growth rate; RTK, receptor tyrosine kinase; TBS, Tris-buffered saline; ANOVA, analysis of variance. BCR, breakpoint cluster region; ABL1, Abelson murine leukemia viral oncogene homolog-1; EML-4, echinoderm microtubule-associated protein–like 4; ALK, anaplastic lymphoma kinase; HCK, hematopoietic cell kinase; BTK, Bruton's tyrosine kinase; AURKA, aurora kinase A.

technologies (4–10). The polypharmacology of kinase inhibitors has resulted in the discovery of new indications for particular compounds. For example, imatinib was initially developed as a BCR-ABL inhibitor for the treatment of chronic myelogenous leukemia, but its activity against c-KIT/PDGFR allowed it to be a successful drug for the treatment of gastrointestinal stromal tumors (11, 12). Similarly, crizotinib was developed as a MET inhibitor, but its activity against ALK resulted in its approval for the treatment of EML4-ALK–positive NSCLC. In several cases, kinase inhibitor polypharmacology has been shown to be important for anticancer activity. For example, the ability of ibrutinib to simultaneously inhibit BTK and HCK makes it a superior drug for treatment of Waldenström's macroglobulinemia as compared with highly selective BTK inhibitors (13). Similarly, sorafenib, originally developed as a BRAF inhibitor, is now known to target numerous other kinases, including VEGFR, PDGFR, RET, DDR1/2, and FLT3 (4), leading to its later approval as a multikinase inhibitor for renal cell carcinoma and hepatocellular carcinoma (14). Similarly, rationally designed inhibitors that simultaneously target bromodomains and kinases have shown superior potency compared with a single target inhibition (15). A recent report suggests that >60% of Food and Drug Administration–approved kinase inhibitors, including sorafenib, dasatinib, pazopanib, and ponatinib, exert their mechanism in a multitargeted manner by targeting at least three or more kinases (16).

With a better understanding of molecular mechanisms governing tumor growth and progression, efforts are underway to rationally design drugs with precision polypharmacology. The most promising efforts combine structure-based analysis with medicinal chemistry campaigns to identify pharmacophores that potently inhibit two or more kinases. Using this approach, Apsel *et al.* (17) developed inhibitors that simultaneously target PI3K and tyrosine kinases to overcome resistance mediated by activation of one or the other signaling kinases. In a study that combined phenotypic and target-based drug discovery approaches, Dar *et al.* (18) identified inhibitors with polypharmacological profiles that exerted potent activity in a RET-kinase driven *Drosophila* model bearing multiple endocrine neoplasia 2.

A major challenge in rationally designing cancer drugs with polypharmacology is to identify the subset of kinases that must be simultaneously inhibited to induce potent antiproliferative effects in a particular tumor type. One way to address this is to conduct systematic phenotypic screens using drug combinations and/or gene knockout techniques (19–24). This approach is complicated by the difficulty of achieving simultaneous knockdown or knockout of multiple targets in a single cell (such multigene knockouts are often lethal). In this study, we demonstrate an alternate strategy that uses a multitargeted kinase inhibitor, SM1-71, with well-characterized polypharmacology as a chemical tool to investigate signaling vulnerabilities in cancer cells. As a proof of concept, we explored signaling vulnerabilities in a KRAS mutant NSCLC cell line, H23-KRAS^{G12C}, and demonstrated that dual inhibition of MEK1/2 and IGF1R/INSR is required for antiproliferative activity in these cells. Our work provides a framework for leveraging a multitargeted kinase inhibitor with known polypharmacology to identify key signaling pathways driving tumor cells. This further lays the path for development of active compounds with desired polypharmacology or effective combination therapies.

Results

Investigating the cytotoxic effect of SM1-71 across multiple cancer cell lines

SM1-71 is a diaminopyrimidine kinase inhibitor that potently targets kinases both through reversible binding in the ATP-binding site and irreversible binding promoted by reaction of the SM1-71 acrylamide moiety with cysteine resides (25, 26) (Fig. 1*a*). We synthesized the reversible analog of SM1-71, SM1-71-R, which lacks the acrylamide warhead and is thus incapable of forming covalent bonds, as a control compound for our studies of cellular effects of SM1-71 (Fig. 1*a*). We previously used chemical proteomic approaches to elucidate ~54 kinase targets of SM1-71 (45) (Table S1) and identified 24 kinases as exhibiting an IC_{50} value <10 μM (Table 1). Thirteen of these kinases have well-annotated functions in promoting cell growth and proliferation, including YES1, SRC, MAP2K2 (MEK2), AURKA, MAP2K1 (MEK1), MAP3K1, MAPK1 (ERK2), MAPK3 (ERK1), WEE1, IGF1R, INSR, DDR1, and MET. Based on the number of proproliferative targets in this list, we sought to determine which of these were important for the antiproliferative activities of SM1-71 using multiple cancer cell lines.

We screened SM1-71 against a panel of cancer cell lines having diverse genotypes and tumor origin. These cells included five NSCLC lines (H23, H460, H1975, HCC827, and H3122) and three triple-negative breast cancer (TNBC) lines (MDA-MB-453, MDA-MB-468, and MDA-MB-231) as well as colon cancer (HCT116), pancreatic ductal adenocarcinoma (MiaPaca2), and melanoma (A375) cell lines (see Table 2 for genotypes). For comparative purposes, we profiled investigational and clinically approved kinase inhibitors against their described nominal targets, including PI3K, MEK1/2, ERK1/2, EGFR, BRAF, ALK, MET, and IGFR1 (Table 3). Cells were plated and 24 h later treated with varying doses of compounds for a period of 72 h. The CellTiter-Glo reagent was added to the plates, which were then analyzed for cytostatic or cytotoxic effects potentially induced by the drugs. To overcome confounding effects of varying division rates between cell lines on estimates of drug potency and efficacy, we used our recently developed growth rate (GR)-corrected values (27, 28). We use GR_{50} as a measure of potency (analogous to IC_{50}) and GR_{max} as a measure of maximal efficacy (analogous to E_{max}; File S1). A GR_{max} value between 1 and 0 corresponds to partial growth inhibition, a value of 0 indicates complete cytostasis, and a negative value denotes cell killing (27). The GR values reported in Table S2 were computed using the online GR Calculator (http://www.grcalculator.org[4]; see "Experimental procedures and Ref. 29).

In eight of 11 cell lines tested, SM1-71 induced potent cytotoxicity with nanomolar values for GR_{50} and negative GR_{max}

[4] Please note that the JBC is not responsible for the long-term archiving and maintenance of this site or any other third party hosted site.

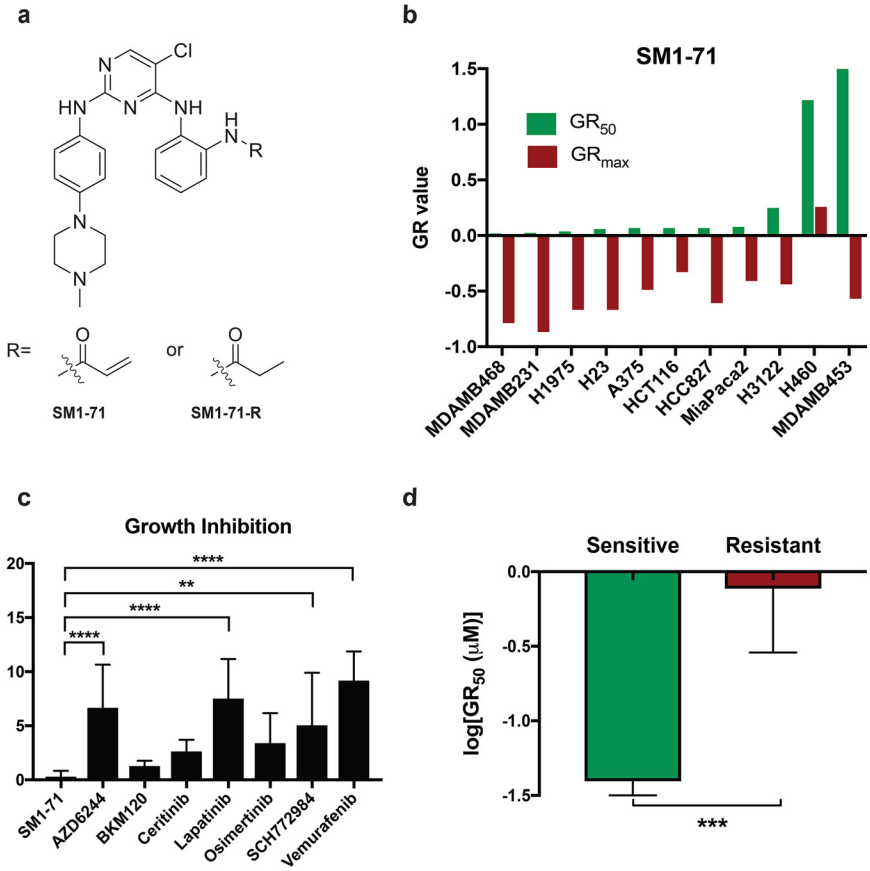

Figure 1. Growth inhibitory screen across multiple cancer cell lines. *a*, chemical scaffold of SM1-71 (covalent inhibitor) and its reversible analog SM1-71-R. *b*, GR_{50} and GR_{max} values from two independent experiments representing growth inhibitory potency of SM1-71 across 11 different cancer cell lines with mutations in KRAS, EGFR, BRAF, ALK, and PIK3CA. A negative GR_{max} value represents cytotoxicity, a GR_{max} value between 0 and 1 indicates partial growth inhibition, and a value equal to 0 represents complete growth arrest. *c*, average growth inhibitory potency (GR_{50}) from two independent experiments across 11 cancer cell lines for SM1-71 and kinase inhibitors targeting MEK (AZD6244), PI3K (BKM120), ALK (ceritinib), EGFR/HER2 (lapatinib), EGFR (osimertinib), ERK (SCH772984), and $BRAF^{V600E}$ (vemurafenib). Statistical analysis was carried out using one-way ANOVA. ****, $p < 0.0001$; **, $p = 0.007$. *d*, comparison of the growth inhibitory potency of SM1-71 ($logGR_{50}$) averaged from two independent experiments across eight sensitive (H23, H1975, HCC827, A375, HCT116, MDA-MB-231, MDA-MB468, and MiaPaca2) and three resistant (H3122, H460, and MDA-MB-453) cell lines. Cells were treated 24 h postplating for 72 h. Statistical analysis was carried out using the two-tailed unpaired *t* test across the $logGR_{50}$ values (***, $p = 0.0005$). All statistical analyses were performed using GraphPad Prism 7.0 software. All GR_{50} and GR_{max} values represent the average of two independent experiments carried out in technical triplicate. *Error bars* represent S.D (mean ± SD).

Table 1

List of kinases inhibited by SM1-71 (IC_{50} value <10 μM) in the multiplexed inhibitor bead (MIB) assay and their role in promoting proliferation

Kinases were identified and reported in Rao *et al.* (45).

Kinase	Binding	Proproliferative?
YES1	Covalent	Yes
SRC	Covalent	Yes
MAP2K2	Covalent	Yes
AURKA	Reversible	Yes
MAP2K1	Covalent	Yes
MAP3K1	Covalent	Yes
MAPK1	Covalent	Yes
MAPK3	Covalent	Yes
WEE1	Reversible	Yes
IGF1R	Reversible	Yes
INSR	Reversible	Yes
DDR1	Reversible	Yes
MET	Reversible	Yes
GAK	Covalent	No
AAK1	Covalent	No
LIMK1	Covalent	No
BMP2K	Covalent	No
TEC	Reversible	No
PTK2	Reversible	No
MARK2	Covalent	No
PRKD3	Reversible	No
LYN	Reversible	No
TGFBR2	Covalent	No
TNIK	Reversible	No

values (Fig. 1*b* and Table S2). SM1-71 was significantly more potent (the GR_{50} value was lower) across all cell lines tested than highly optimized inhibitors of MEK1/2 (AZD6244), PI3K (BKM120), ALK (ceritinib), EGFR (osimertinib), EGFR and HER2 (lapatinib), ERK1/2 (SCH772984), and BRAF (vemurafenib) ($p < 0.01$; Fig. 1*c*). In three of 11 lines (H3122, H460, and MDA-MB-453), SM1-71 was comparatively less potent, with GR_{50} ranging from 0.25–1.5 μM (Fig. 1*b*). Based on these data, eight lines were classified as SM1-71–sensitive, and three were classified as resistant ($p = 0.0005$, difference in potency between sensitive and resistant cell lines) (Fig. 1*d*). These results indicate that SM1-71 is broadly active on cancer cell lines and suggest that multitargeted agents exhibit improved cytotoxicity compared with highly optimized inhibitors.

Elucidating kinases responsible for mediating cytotoxic effects in KRAS mutant cells

From our growth inhibitory screen, we identified several cancer cell lines with different genetic backgrounds that were highly sensitive to SM1-71 while showing resistance to inhibitors designed to target single kinases. To demonstrate that SM1-71 serves as an effective multitargeted chemical tool com-

Table 2
Cell lines used in the growth inhibitory screens

Cell line	Tumor type	Mutation
H23	Lung	$KRAS^{G12C}$, TP53
H358	Lung	$KRAS^{G12C}$
H460	Lung	$KRAS^{Q61K}$, $PIK3CA^{E545K}$, CDKN2A
H1792	Lung	$KRAS^{G12C}$, TP53
Calu-1	Lung	$KRAS^{G12C}$
Calu-6	Lung	$KRAS^{Q61K}$, TP53
H1975	Lung	$EGFR^{L858R/T790M}$, CDKN2A, $PIK3CA^{G118D}$, TP53
HCC827	Lung	$EGFR^{delE746\text{-}A750}$
H3122	Lung	EML4-ALK rearrangement
HCT116	Colon	$KRAS^{G13D}$, CTNNB1, CDKN2A, $PIK3CA^{H1047R}$
Mia-Paca-2	Pancreas	$KRAS^{G12C}$, CDKN2A, TP53
MDA-MB-231	Breast	$KRAS^{G13D}$, $BRAF^{G464V}$, TP53, CDKN2A, NF2
MDA-MB-468	Breast	PTEN, RB1, SMAD4, TP53
MDA-MB-453	Breast	$PIK3CA^{H1047R}$
A375	Melanoma	$BRAF^{V600E}$, CDKN2A

Table 3
List of clinical and investigational kinase inhibitors used in the study

Compound	Nominal targets
AZD6244	MEK1/2
SCH772984	ERK1/2
BKM120	Pan-PI3K
Osimertinib	EGFR
Lapatinib	EGFR/HER2
Ceritinib	ALK
Vemurafenib	$BRAF^{V600E}$
AEW541	IGF1R
Crizotinib	MET/ALK

pound for revealing key signaling pathways driving growth and proliferation, we chose a single sensitive cell line to carry out further experimental analyses. We were especially interested in elucidating druggable targets in KRAS mutant cells because RAS mutations are found across different tumors and lack effective targeted therapy (30, 31). We carried out all our analyses in H23-$KRAS^{G12C}$ NSCLC cells, which we recently employed to generate a global map of kinases to which SM1-71 binds (45). To identify kinase targets of SM1-71 responsible for mediating cytotoxic effects in H23-$KRAS^{G12C}$ cells, we measured the phosphorylation status of kinases involved in MAPK and PI3K signaling pathways, two effectors downstream of KRAS, using Western blotting (Fig. 2*a*; see Fig. S1 for blots from two independent experiments). H23-$KRAS^{G12C}$ cells were treated with 1 μM SM1-71 or SM1-71-R (reversible analog) for a period of 2 h followed by drug washout and replacement with fresh medium. Cells were collected and lysed 0, 2, and 4 h postwashout to distinguish between transient and reversible and prolonged and potentially irreversible inhibition by SM1-71 (SM1-71 can covalently bind to kinases such as MEK1/2, ERK1/2, SRC, etc. (45)). To further distinguish between reversible and irreversible inhibition, we performed treatment–washout experiments using SM1-71-R, which cannot form covalent adducts. We found that SM1-71 was potent as an inhibitor of phosphorylation on p-AKT^{S473} and p-$ERK1/2^{T202/Y204}$ prior to washout (at $t = 0$ h) (Fig. 2*a*). Inhibition of p-$ERK1/2^{T202/Y204}$ was sustained 2 h postwashout. SM1-71-R resulted in inhibition of phosphorylation of only p-AKT^{S473}. We observed a concomitant increase in p-$MEK1/2^{S217/S221}$ levels after 2 and 4 h postwashout, which is common following ERK1/2 inhibition as a consequence of disrupting negative feedback regulation (32). We observed p-AKT^{S473} and p-$ERK1/2^{T202/Y204}$ levels rising 2 and 4 h postwashout with SM1-71 and SM1-71-R. Several reports have previously shown that kinases within the MAPK and PI3K pathways are reactivated in response to specific inhibitors that suppress negative feedback loops (33–35). We thus predict a similar phenomenon responsible for the reactivation of p-AKT^{S473} and p-$ERK1/2^{T202/Y204}$ signaling upon treatment with SM1-71 and SM1-71-R.

So far, signaling analysis using Western blotting demonstrated direct cellular inhibition of MAPK and PI3K signaling pathways. Our data also revealed inhibition of p-AKT^{S473} (PI3K pathway), which was likely affected through inhibition of an upstream receptor and not directly by targeting PI3K, AKT, or mTOR (nontargets of SM1-71; Table S1). To test this possibility, we profiled a panel of 49 receptor tyrosine kinases (RTKs) using an RTK array (R&D Systems) in which phosphorylation of RTKs (and their inhibition in the presence of SM1-71) was measured by exposing cell lysates to capture antibodies spotted in duplicates (per RTK) on a nitrocellulose membrane (see Fig. S2 for dot-blots from the two independent experiments). H23-$KRAS^{G12C}$ cells were treated with 1 μM SM1-71 or DMSO for 6 h and lysed after which the lysate was incubated with the RTK arrays. Phosphorylation signals were quantified for both the SM1-71– and DMSO-treated samples using the dot-blot analyzer (ImageJ software), and -fold change was calculated. These -fold change values were averaged across two independent experiments to generate an average -fold change signal (±S.E.) for each RTK. These average -fold change values for IGF1R (80-fold), INSR (12-fold), and MET (5-fold) have been plotted as bar graphs (Fig. 2*b*) ($p < 0.0001$, compared with INSR and MET -fold change). Our results indicate that among the 49 RTKs profiled, SM1-71 potently inhibited IGF1R, INSR, and MET. We conclude that SM1-71 is active on at least three RTKs known to lie upstream of the PI3K signaling pathway. Furthermore, we identified each of these three RTKs, IGF1R, INSR, and MET, as direct targets of SM1-71 from our previous study (Table S1) (45).

Validation of key targets driving proliferation in H23-$KRAS^{G12C}$ cells

To determine whether inhibition of IGF1R/INSR and/or MET is involved in down-regulation of p-AKT^{S473} levels, we attempted to phenocopy the effects using combinations of kinase inhibitors. The effects of 1 μM SM1-71 were compared with those of an ALK/MET inhibitor (1 μM crizotinib), IGF1R inhibitor (AEW541), ERK1/2 inhibitor (SCH772984), pan-PI3K inhibitor (BKM120), or DMSO. H23-$KRAS^{G12C}$ cells were incubated with the compound for 4 h, and phosphorylation of downstream kinases was assessed using Western blotting (Fig. 2*c*; see Fig. S3 for blots from two independent experiments). We found that crizotinib reduced p-$MET^{Y1234/1235}$ phosphorylation to background levels, partially reduced p-AKT^{S473} levels but had no discernable effect on p-$ERK1/2^{T202/Y204}$ levels. AEW541 reduced p-IGF1R/p-$INSR^{Y1135/1136}$ levels and caused complete inhibition of pAKT^{S473}, also with no effect on p$ERK1/2^{T202/Y204}$ (Fig. 2*c*). This inhibition of IGF1R/INSR and/or MET in H23-$KRAS^{G12C}$ cells can down-regulate the PI3K pathway without affecting the activity of the MAPK pathway. In contrast, SM1-71 reduced not only p-IGF1R/p-$INSR^{Y1135/1136}$ and p-$MET^{Y1234/1235}$ levels but also p-ERK1/

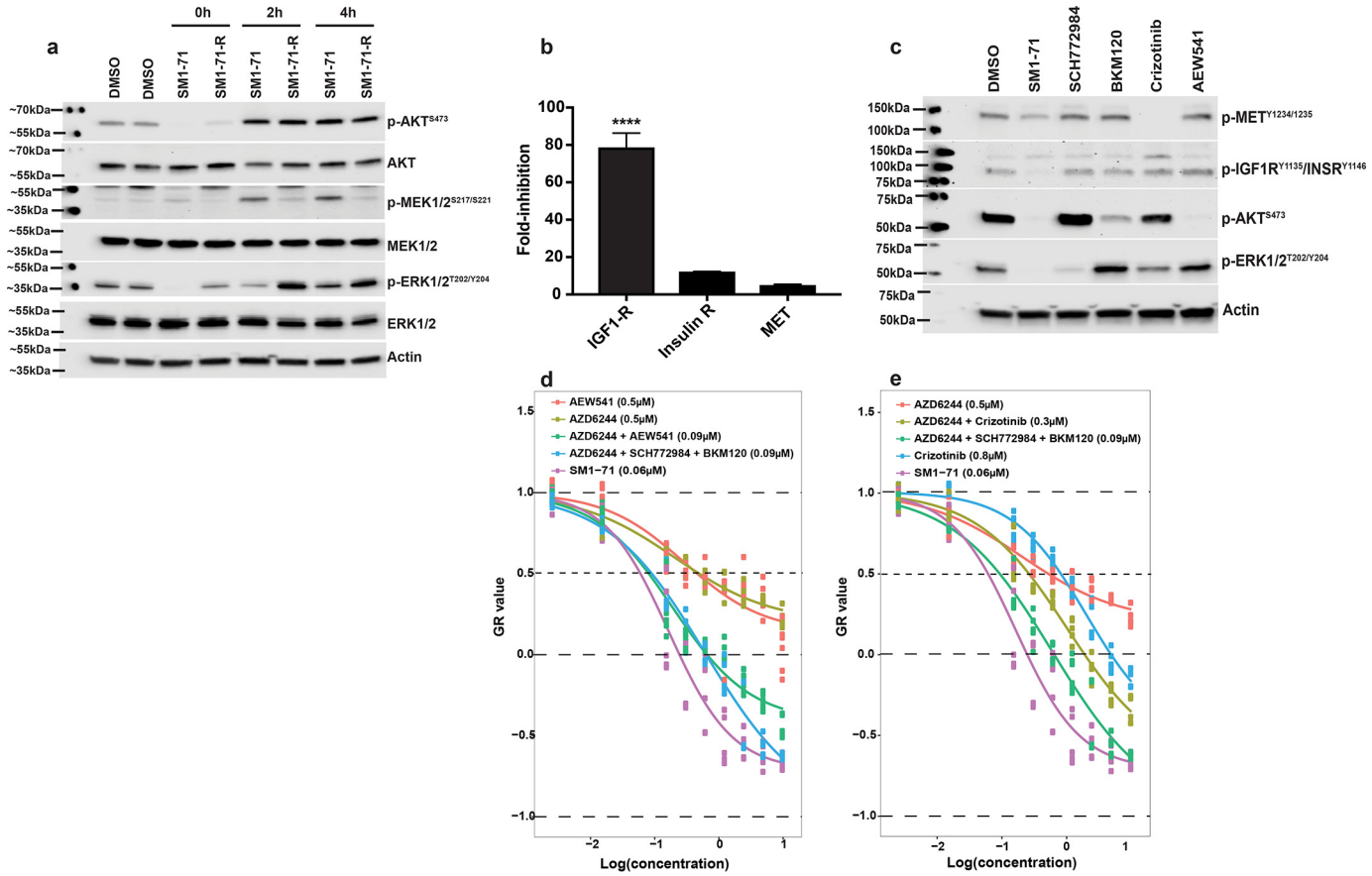

Figure 2. Characterizing the mechanism of SM1-71–associated cytotoxicity in H23-KRAS^{G12C} cells. *a*, Western blot analysis of phosphorylation of kinases in cells treated with 1 μM SM1-71, SM1-71-R, or DMSO for 2 h followed by drug washout, replacement with fresh drug-free medium, and subsequent lysis 0, 2, and 4 h postwashout. The blot shown is from one of two independent experiments performed (see Fig. S1 for both blots). *b*, phospho-RTK inhibition following treatment with 1 μM SM1-71 for 6 h. RTK array blots from two independent experiments were quantified, and average -fold inhibition (±S.E.) for SM1-71– and DMSO-treated samples has been represented in the bar graph. Statistical significance was carried out using one-way ANOVA on GraphPad Prism 7.0. Dot-blots for each array are shown in Fig. S2, $p < 0.0001$ is the significant difference in fold-change between IGF1R and MET and IGF1R and INSR. *c*, Western blot analysis of p-MET$^{Y1234/1235}$, p-IGF1R/p-INSR$^{Y1135/1136}$, p-AKT^{S473}, and p-ERK1/2$^{T202/Y204}$ treated with 1 μM SM1-71, SCH772984 (ERK), BKM120 (PI3K), crizotinib (MET), AEW541 (IGF1R), or DMSO for 4 h. The blot shown is from one of two independent experiments performed (please refer to Fig. S3 to see blots from both experiments). *d* and *e*, growth inhibition assay in H23-KRAS^{G12C} cells treated with SM1–71, AZD6244 (MEK), AEW541, crizotinib, or equimolar combinations of inhibitors (GR_{50} values indicated within *parentheses*). Cells were treated 24 h postplating for 72 h. The GR_{50} values represent the average of two independent experiments carried out in triplicate. Each point on the growth inhibition curve represents the average of two independent experiments carried out in technical triplicate ±S.E.

$2^{T202/Y204}$. We therefore asked whether inhibition of MEK1/2 in combination with IGF1R/INSR or MET would recapitulate the cytotoxicity observed with SM1-71. We found that AZD6244 (MEK1/2 inhibitor) and AEW541 were weakly cytostatic on their own (GR_{50} = 0.5 μM; GR_{max}, between 0 and 1) but when combined were 5-fold more potent (GR_{50} = 0.08 μM) and also cytotoxic as indicated by a GR_{max} value of −0.4 (Fig. 2*d* and File S1). As previously mentioned, a negative GR_{max} value is indicative of cytotoxicity. Moreover, the MEK–IGFR1 inhibitor combination of AEW541 plus AZD6244, MEK–ERK–PI3K triple-inhibitor combination of AZD6244 plus SCH772984 plus BKM120, and SM1-71 were all similar in potency and cytotoxicity. In contrast, the MEK–MET inhibitor combination of AZD6244 plus crizotinib was only weakly cytotoxic (Fig. 2*e* and File S1). Based on these data, we propose that MEK1/2 and IGF1R/INSR are critical drivers of growth and proliferation in H23-KRAS^{G12C} cells. Furthermore, these are targeted by SM1-71, which results in inhibition of proliferation and induction of cell death.

Distinct molecular mechanisms drive different tumor types

The multitargeted nature of SM1-71 makes it a valuable tool to interrogate cancer cell signaling across different cell lines and tumor types. Having investigated pathways responsible for driving growth in a sensitive cell line (H23-KRAS^{G12C}), we wished to further apply SM1-71 to understand what might be mediating resistance in some other cell lines. From our growth inhibitory screen, we identified H3122, H460, and MDA-MB-453 cells to be slightly more resistant (submicromolar/micromolar GR_{50} values compared with nanomolar values for sensitive cell lines) to the action of SM1-71. H3122 is an NSCLC line harboring an EML4-ALK translocation in which exposure to ceritinib, an ALK inhibitor, strongly inhibits proliferation (GR_{50} = 0.05 μM, GR_{max} = −0.78; Fig. 3*a* and Table S2). However, SM1-71 binds only weakly to the ALK oncogenic driver (data not shown). The H460 NSCLC cell line and the MDA-MB-453 TNBC cell line both harbor E545K and H1074R mutations in the PIK3CA gene (https://cancer.sanger.ac.uk/cosmic).[4] This

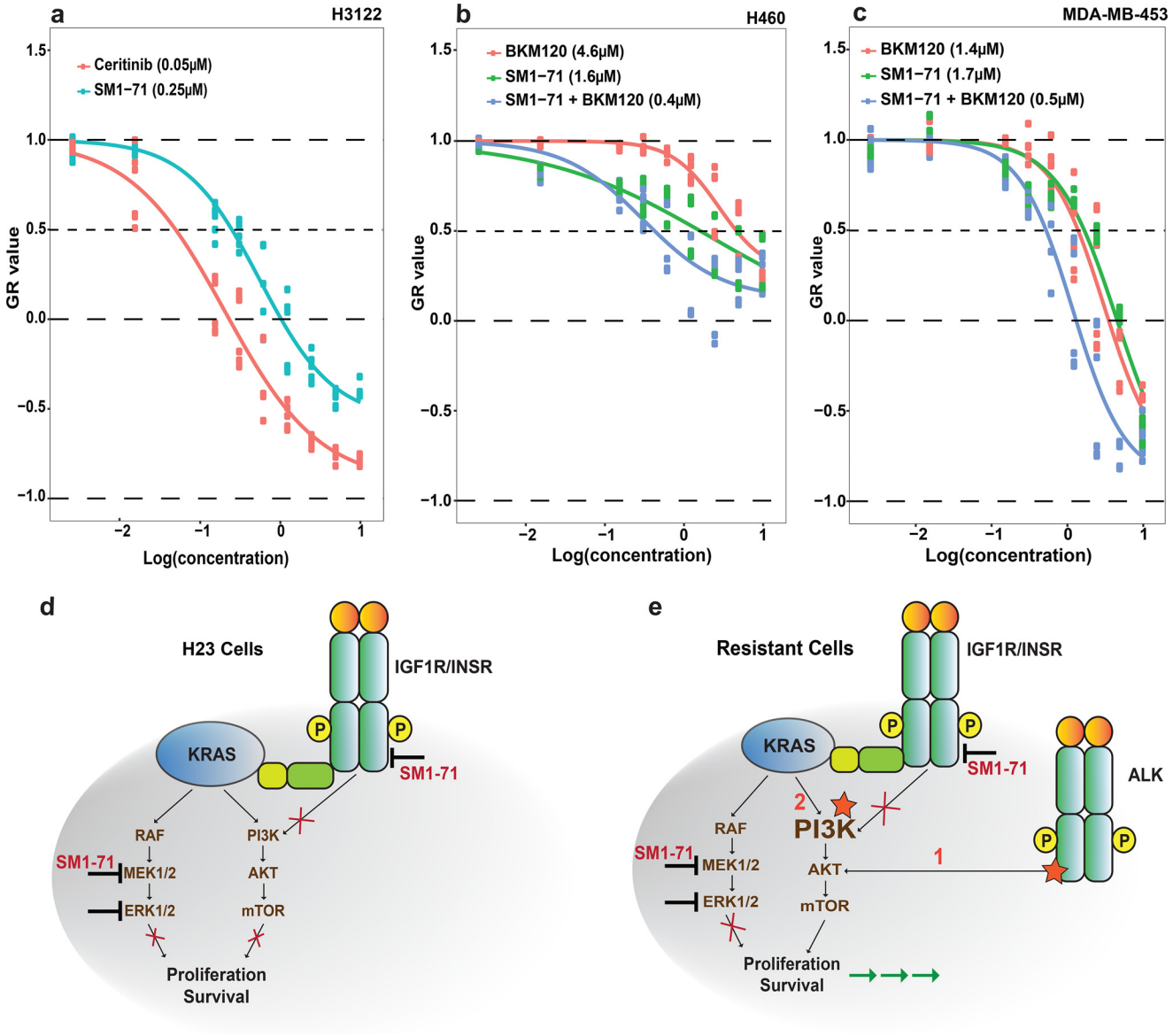

Figure 3. Evaluating cell line–dependent polypharmacology associated with SM1-71. *a*, growth inhibitory potency of SM1-71 and ceritinib in the EML4-ALK–positive H3122 NSCLC cells. *b* and *c*, growth inhibitory potency induced by SM1-71, BKM120 (PI3K inhibitor), or their equimolar combination in the PIK3CA mutant H460 NSCLC (*b*) and MDA-MB-453 TNBC (*c*) cell lines. Each point on the growth inhibition curves represent the average of two independent experiments carried out in technical triplicate ±S.E. Average GR_{50} values from two independent experiments have been shown for *a*–*c*. *d*, proposed mechanism of action of cytotoxicity in H23-$KRAS^{G12C}$ cells by simultaneously inhibiting IGF1R/INSR and MEK1/2. *e*, proposed mechanisms to enhance potency in resistant cells by targeting the driver oncogene EML4-ALK (mechanism 1) or by blocking activating PI3K signaling (mechanism 2).

mutation introduces an oncogenic driver downstream of the RTKs such as IGF1R/INSR, which activates the PI3K pathway. We therefore predicted that a pan-PI3K inhibitor such as BKM120 would make these cell lines sensitive to SM1-71. We found that the combination of SM1-71 plus BKM120 reduced the GR_{50} for SM1-71 >3-fold in both cell lines, suggesting that resistance is possibly a consequence of PIK3CA mutation (Fig. 3, *b* and *c*). Of note, both HCT116 and H1975 harbor H1074R and G118D PIK3CA mutations, respectively, and were sensitive to SM1-71. This suggests that the PIK3CA mutation is not a sufficient oncogenic driver to confer SM1-71 resistance. Such cell line–specific differences are observed with many kinase inhibitors and arise from the specific signaling biology of the lines (36, 37). However, because SM1-71 has multiple targets, we cannot fully exclude other mechanisms that might be contributing toward the overall sensitivity and resistance effects of the compound.

Discussion

Several challenges, including complex signaling networks, cross-talk with the tumor microenvironment, and onset of drug resistance, are associated with treating cancers driven by multiple oncogenes. It is thus increasingly appreciated that only use of drugs that affect multiple signaling nodes will result in strong antiproliferative effects and delay the onset of drug resistance. Such compounds, referred to as polypharmacological drugs, have been investigated in the past to treat polygenic diseases such as cancers, CNS disorders, and inflammatory disorders. Our current work aims to promote the rational development of such inhibitors by developing means to unravel key signaling

pathways that must be simultaneously inhibited to achieve maximum antitumor effects. By utilizing a multitargeted kinase inhibitor, SM1-71, that serves as an effective tool compound we were able to elucidate molecular mechanisms driving specific cancer cell types. In our previous study, we used SM1-71 to interrogate the human kinome to identify cysteines that can be targeted because of the covalent nature of the compound (45). In the present study, we extended the use of this compound to the investigation of signaling pathways that drive cellular proliferation in cancer cells. As a proof of concept, we demonstrated the utility of this chemical tool by using a KRAS mutant NSCLC cell line, H23-KRAS^{G12C}, and identified MEK1/2 and IGF1R/INSR as being key players in driving cellular proliferation. We corroborated our findings by using clinical and investigational kinase inhibitors to induce pharmacologic shutdown of kinases. Our results validated that dual inhibition of MEK1/2 and IGF1R/INSR led to down-regulation of the MAPK and PI3K pathways, which is responsible for inducing potent cytotoxic effects in H23-KRAS^{G12C} cells. Our findings are further supported by the knowledge that mutant KRAS leads to constitutive activation of its downstream effector pathways, MAPK and PI3K, and thus, inhibiting both arms of the oncogene leads to potent antitumor effects (38–40). Furthermore, preclinical and clinical studies focusing on the dual inhibition of MEK1/2 and IGF1R/INSR have demonstrated beneficial effects across different types of cancers (41–44). Our study does not unequivocally prove the pharmacologically relevant targets of SM1-71; indeed, the functionally relevant targets of this compound are likely different in different cell types.

It is well established that for drugs that target a single oncogene (*e.g.* EGFR, BCR-ABL, BTK, etc.), gene knockout (*e.g.* RNAi or CRISPR-Cas9) or rescue experiments following site-directed mutagenesis that prevents the drug from binding the kinase are powerful techniques to functionally validate the on-target effect of the drug. However, in the case of polypharmacological agents acting on polygenic tumors, similar methods pose many challenges (3). An alternative strategy is to use combinations of selective inhibitors targeting kinases that phenocopy the effects induced by a polypharmacological inhibitor. Given the multitargeted properties of SM1-71, we adapted a similar strategy to pharmacologically validate potential targets.

Our study also draws attention to the benefits of using a multitargeted chemical probe compared with a selective chemical probe. Traditionally, most chemical probes are designed to retain selectivity and specificity toward a single target to characterize its role in a given cell type. However, in our current study, we demonstrate that chemical probes with multiple targets can serve as powerful tools to interrogate oncogenic drivers in cancer cells in lieu of systematic combinatorial screens. By using a combination of cell-based assays and pharmacologic inhibitors, we outlined a framework for adopting multitargeted kinase inhibitors with defined polypharmacology as effective chemical probes. As a proof of concept, we conducted all our analyses in the sensitive H23-KRAS^{G12C} cells; however, a similar strategy can be adopted to interrogate other cell types. In fact, we demonstrated this by extending our evaluation toward three cell lines that were relatively resistant to SM1-71 in the growth inhibitory screen. Further investigation is required to ascertain these mechanisms as causes for the lowered activity of SM1-71 in these less sensitive cell lines. Nonetheless, direct pharmacologic inhibition of targets provides compelling evidence toward the mechanism of cytotoxicity in both sensitive and resistant cells. Together, these illustrate the generalizability of this approach and imply that such probes can serve as effective means to elucidate signaling pathways driving tumor cells.

Polypharmacological agents are also associated with several limitations when it involves improving their properties through systematic medicinal chemistry efforts. It can be extremely difficult to hone potency and selectivity toward two or more desired targets while simultaneously achieving selectivity and the desired pharmacokinetic and toxicological profile. A further challenge relates to finding suitable experimental models that can faithfully predict response in the clinic. For example, a simple cell proliferation assay may be able to predict response to a BCR-ABL inhibitor but may be a poor predictor for a kinase inhibitor such as SM1-71 that inhibits through multiple targets. Specifically, in the case of SM1-71, the ability of the compound to block PI3K pathway signaling through RTK inhibition may not be accurately modeled in simple cancer cell proliferation assays with unnatural levels of growth factors. Given that polypharmacological kinase inhibitors will continue to be discovered, we propose that these multitargeted inhibitors can serve as effective research tools to help unravel pathways that must be targeted. Their application for path finding and vulnerability identification will allow the development of rational combinations as well as potentially aide rational design of tailored polypharmacology agents.

Materials and methods

Cell culture

Cell lines used in the study included NSCLC cells H23 (KRAS^{G12C}), H460 (KRAS^{Q61H}/PIK3CA^{E545K}), H1975 (EGFR$^{L858R/T790M}$/CDKN2A/PIK3CA^{G118D}/TP53), HCC827 (EGFR$^{delE746\text{-}A750}$), and H3122 (EML4-ALK rearrangement); TNBC cells MDA-MB-453 (PIK3CA^{H1047R}), MDA-MB-468 (PTEN/RB1/SMAD4/TP53), and MDA-MB-231 (KRAS/BRAF/TP53/CDKN2A); colorectal cells HCT116 (KRAS^{G13D}/CTNNB1/CDKN2A/PIK3CA^{H1047R}); pancreatic cells MiaPaca2 (KRAS^{G12C}/CDKN2A/TP53); and melanoma cells A375 (BRAF^{V600E}/CDKN2A). All the NSCLC cell lines were a generous gift from Dr. Pasi Janne (Dana-Farber Cancer Institute, Boston, MA). Cell lines were tested for mycoplasma contamination (Lonza MycoAlert kit, catalog number LT07-318) and authenticated using short tandem repeat profiling (Molecular Diagnostics Laboratory, Dana-Farber Cancer Institute, Boston, MA). NSCLC cell lines were maintained in RPMI 1640 medium (30-2001, ATCC); TNBC, MiaPaca2, and A375 cell lines were maintained in Dulbecco's modified Eagle's medium (10-013-CV, Corning); and HCT116 cells were maintained in McCoy's 5A medium (30-2007, ATCC). All media were supplemented with 10% heat-inactivated fetal bovine serum (Gibco) and 1% penicillin/streptomycin (30-002-Cl, Corning). Cells were grown in incubators maintained at 37 °C and 5% CO_2.

Chemical synthesis

Detailed methodology on the synthesis of compounds has been described previously (25).

Growth inhibition assay

Cells were plated in 384-well plates (3764, Corning) at a seeding density of 2000 cells/well using the Multidrop Combi Reagent Dispenser (Thermo Fisher Scientific). Cells were treated with different doses of compounds for 72 h using the automated HP-D300 digital dispenser and normalized to 0.2% DMSO 24 h postplating. Viability was measured 72 h after treatment by adding 25 μl/well CellTiter-Glo (G7572, Promega) and reading plates using the Synergy H1 microplate reader (BioTek). Each experiment was carried out in technical triplicate and biological duplicate.

Growth inhibition analysis using the online GR calculator

Growth inhibition across cell lines was analyzed using the online GR calculator (http://www.grcalculator.org/grcalculator)[4] developed by members of the LINCS-BD2K Data Coordination and Integration Center, Harvard Medical School (29), which is based on the method originally described by Hafner *et al.* (27). The GR metrics (GR_{50} and GR_{max}) along with their corresponding IC_{50} values were calculated using the online GR calculator based on cell division rates obtained for different cell lines. To measure cell doubling time, cells were seeded at an initial count of 500,000 in a 10-cm dish, and final count was measured 3–4 days (72–96 h) later using the TC20 automated cell counter (Bio-Rad). The doubling time was calculated using the following formula: $DT = T\ln(2)/\ln(Xe/Xb)$ where T is the time of growth (hours), Xe is the final cell count, and Xb is the initial cell count. The following doubling times were used: A375 (19.2 h), H1975 (31.8 h), H23 (40.6 h), H3122 (32.5 h), H460 (20.7 h), HCC827 (29.7 h), HCT116 (20.4 h), MDA-MB-231 (44.5 h), MDA-MB-453 (41.8 h), MDA-MB-468 (35.3 h), and MiaPaca2 (31.3 h). Data from the CellTiter-Glo assay along with cell division rates were uploaded onto the online GR calculator that generated dose-response curves and GR_{50} and GR_{max} values along with all other statistical parameters that can be found in File S1. Codes used in the analysis can be made available upon request.

Western blotting

H23-KRAS^{G12C} cells were grown in 10-cm dishes and treated with the given concentrations of compounds or DMSO for 2–6 h. For the washout experiments, cells were washed twice with PBS followed by the addition of fresh medium. Cells were then lysed at different time points postwashout. In the case of non-washout experiments, cells were lysed right after treatment following quick rinses with cold PBS. Lysis was carried out using 300 μl/dish cold M-PER Mammalian Protein Extraction Reagent (78505, Thermo Fisher Scientific) substituted with 100× HALT protease and phosphatase inhibitor (final concertation, 1×) (78446, Thermo Fisher Scientific). After 30 min of incubation on ice (with rocking), lysate was centrifuged at 14,800 rpm for 15–20 min at 4 °C. The supernatant (protein extract) was collected and quantified using the Micro BCA Protein Assay kit (23235, Thermo Fisher Scientific). Samples were prepared by adding 2×–4× Laemmli sample buffer (161-0737 and 161-0747, Bio-Rad) substituted with 2-mercaptoethanol (5%, v/v) (Sigma-Aldrich) and boiling at 95 °C for at least 10 mins. Gel electrophoresis was performed using Precast Protein Gels (4569034 and 4569036, Bio-Rad) loaded with 10–20 μg of protein/well. Proteins were transferred onto polyvinylidene difluoride membranes (0.45-μm pore size; Novex Life Technologies). 5% nonfat dry milk (9999S, Cell Signaling Technology) in Tris-buffered saline (TBS) substituted with 0.1% Tween (TBST) solution was used as the blocking buffer and to prepare antibody solutions. Buffers used included 10× running (Tris/glycine/SDS buffer, 161-0772, Bio-Rad), 10× transfer (35040, Thermo Fisher Scientific), and 20× TBS (sc-362305, Santa Cruz Biotechnology). We purchased antibodies from Cell Signaling Technology for the following: p-MEK1/2^{S221} (2338S; rabbit), MEK1/2 (9126S; rabbit), p-ERK1/2$^{T202/Y204}$ (4370S; rabbit), ERK1/2 (4696S; mouse), p-MET$^{Y1234/1235}$ (3077S; rabbit), MET (3148S; mouse), p-IGF1R/p-INSR$^{Y1135/1136}$ (3024S; rabbit), IGF1R (9750S; rabbit), p-AKT^{S473} (4060S; rabbit), and AKT (4685S; rabbit). Primary antibodies were diluted to a final concentration of 1:1000, and we used a 1:10,000 concentration for secondary antibodies (Cell Signaling Technology). We purchased β-actin antibody from Santa Cruz Biotechnology (sc-47778; mouse); it used at a concentration of 1:5000. We incubated blots with SuperSignal West Dura Extended Duration Substrate (34076, Thermo Fisher Scientific) and visualized them using the myECL imager (Thermo Fisher Scientific). Each experiment was carried out twice; representative blots from a single experiment are shown in Fig. 2, *a* and *c*; and both blots are shown in Figs. S1 and S3.

RTK array

H23-KRAS^{G12C} cells were grown in 10-cm dishes, treated with 1 μM SM1-71 or DMSO for 6 h, washed, extracted, and lysed as described under "Western blotting." Following protein quantification, 500 μg of protein/sample was used to carry out the phospho-RTK array analysis according to the protocol described by the manufacturer (ARY001B, R&D Systems). Henceforth, all incubation and wash steps were accompanied by end-to-end rocking. Briefly, each array was incubated with 2 ml of Array Buffer 1 for 1 h at room temperature. After removal of this blocking buffer, 500 μg of sample diluted in 1.5 ml of Array Buffer 1 was added to each array and incubated overnight at 4 °C. Following washes with 1× Wash Buffer, arrays were incubated with 2 ml of anti-phosphotyrosine-HRP antibody diluted in Array Buffer 2 for 2 h at room temperature. Wash steps were repeated, and arrays were visualized by adding a 1:1 ratio of the SuperSignal West Dura Extended Duration Substrate and scanning them using the myECL imager. Phosphorylation signals obtained were mapped to their respective RTKs using the reference RTK coordinates included in the kit (blots for both experiments are shown in Fig. S2). The experiment was repeated twice, and the phosphorylation signals for each RTK were quantified using the dot-blot analyzer macro in the ImageJ 1.50i software (code and documentation are available upon request). Each phospho-RTK signal had two representative spots on a given array. Fold change was calculated for SM1-71-

and DMSO-treated samples for each RTK and averaged across the two independent experiments. These fold change values ±S.E. were plotted as bar graphs for IGF1R, INSR, and MET. The GraphPad Prism 7.0 software was used to generate graphs and carry out statistical analysis.

Statistical analysis

All statistical analyses were carried out using GraphPad Prism 7.0 software. In Figs. 1*c* and 2*b*, statistical analysis was carried out using one-way ANOVA. In Fig. 1*d*, statistical significance between the sensitive and resistant cell lines was calculated using the two-tailed unpaired *t* test ($p = 0.0005$).

Author contributions—S. R., P. K. S., and N. S. G. conceptualization; S. R., M. H., and K. S. formal analysis; S. R. validation; S. R. and G. D. investigation; S. R. visualization; S. R. and G. D. methodology; S. R. writing-original draft; G. D., M. H., K. S., P. K. S., and N. S. G. writing-review and editing; M. H. and K. S. software; P. K. S. and N. S. G. resources; P. K. S. and N. S. G. supervision; P. K. S. and N. S. G. funding acquisition.

References

1. Ferguson, F. M., and Gray, N. S. (2018) Kinase inhibitors: the road ahead. *Nat. Rev. Drug Discov.* **17,** 353–377 CrossRef Medline
2. Proschak, E., Stark, H., and Merk, D. (2019) Polypharmacology by design: a medicinal chemist's perspective on multitargeting compounds. *J. Med. Chem.* **62,** 420–444 CrossRefMedline
3. Roth, B. L., Sheffler, D. J., and Kroeze, W. K. (2004) Magic shotguns versus magic bullets: selectively non-selective drugs for mood disorders and schizophrenia. *Nat. Rev. Drug Discov.* **3,** 353–359 CrossRef Medline
4. Kitagawa, D., Yokota, K., Gouda, M., Narumi, Y., Ohmoto, H., Nishiwaki, E., Akita, K., and Kirii, Y. (2013) Activity-based kinase profiling of approved tyrosine kinase inhibitors. *Genes Cells* **18,** 110–122 CrossRef Medline
5. Lemeer, S., Zörgiebel, C., Ruprecht, B., Kohl, K., and Kuster, B. (2013) Comparing immobilized kinase inhibitors and covalent ATP probes for proteomic profiling of kinase expression and drug selectivity. *J. Proteome Res.* **12,** 1723–1731 CrossRef Medline
6. Remsing Rix, L. L., Rix, U., Colinge, J., Hantschel, O., Bennett, K. L., Stranzl, T., Müller, A., Baumgartner, C., Valent, P., Augustin, M., Till, J. H., and Superti-Furga, G. (2009) Global target profile of the kinase inhibitor bosutinib in primary chronic myeloid leukemia cells. *Leukemia* **23,** 477–485 CrossRef Medline
7. Munoz, L. (2017) Non-kinase targets of protein kinase inhibitors. *Nat. Rev. Drug Discov.* **16,** 424–440 CrossRef Medline
8. Médard, G., Pachl, F., Ruprecht, B., Klaeger, S., Heinzlmeir, S., Helm, D., Qiao, H., Ku, X., Wilhelm, M., Kuehne, T., Wu, Z., Dittmann, A., Hopf, C., Kramer, K., and Kuster, B. (2015) Optimized chemical proteomics assay for kinase inhibitor profiling. *J. Proteome Res.* **14,** 1574–1586 CrossRef Medline
9. Bantscheff, M., Eberhard, D., Abraham, Y., Bastuck, S., Boesche, M., Hobson, S., Mathieson, T., Perrin, J., Raida, M., Rau, C., Reader, V., Sweetman, G., Bauer, A., Bouwmeester, T., Hopf, C., *et al.* (2007) Quantitative chemical proteomics reveals mechanisms of action of clinical ABL kinase inhibitors. *Nat. Biotechnol.* **25,** 1035–1044 CrossRef Medline
10. Golkowski, M., Brigham, J. L., Perera, G. K., Romano, G. E., Maly, D. J., and Ong, S. E. (2014) Rapid profiling of protein kinase inhibitors by quantitative proteomics. *Medchemcomm* **5,** 363–369 CrossRef Medline
11. Cohen, M. H., Farrell, A., Justice, R., and Pazdur, R. (2009) Approval summary: imatinib mesylate in the treatment of metastatic and/or unresectable malignant gastrointestinal stromal tumors. *Oncologist* **14,** 174–180 CrossRef Medline
12. Dagher, R., Cohen, M., Williams, G., Rothmann, M., Gobburu, J., Robbie, G., Rahman, A., Chen, G., Staten, A., Griebel, D., and Pazdur, R. (2002) Approval summary: imatinib mesylate in the treatment of metastatic and/or unresectable malignant gastrointestinal stromal tumors. *Clin Cancer Res.* **8,** 3034–3038 Medline
13. Yang, G., Buhrlage, S. J., Tan, L., Liu, X., Chen, J., Xu, L., Tsakmaklis, N., Chen, J. G., Patterson, C. J., Brown, J. R., Castillo, J. J., Zhang, W., Zhang, X., Liu, S., Cohen, P., *et al.* (2016) HCK is a survival determinant transactivated by mutated MYD88, and a direct target of ibrutinib. *Blood* **127,** 3237–3252 CrossRef Medline
14. Wilhelm, S. M., Adnane, L., Newell, P., Villanueva, A., Llovet, J. M., and Lynch, M. (2008) Preclinical overview of sorafenib, a multikinase inhibitor that targets both Raf and VEGF and PDGF receptor tyrosine kinase signaling. *Mol. Cancer Ther.* **7,** 3129–3140 CrossRef Medline
15. Ciceri, P., Müller, S., O'Mahony, A., Fedorov, O., Filippakopoulos, P., Hunt, J. P., Lasater, E. A., Pallares, G., Picaud, S., Wells, C., Martin, S., Wodicka, L. M., Shah, N. P., Treiber, D. K., and Knapp, S. (2014) Dual kinase-bromodomain inhibitors for rationally designed polypharmacology. *Nat. Chem. Biol.* **10,** 305–312 CrossRef Medline
16. Wu, P., Nielsen, T. E., and Clausen, M. H. (2016) Small-molecule kinase inhibitors: an analysis of FDA-approved drugs. *Drug Discov. Today* **21,** 5–10 CrossRef Medline
17. Apsel, B., Blair, J. A., Gonzalez, B., Nazif, T. M., Feldman, M. E., Aizenstein, B., Hoffman, R., Williams, R. L., Shokat, K. M., and Knight, Z. A. (2008) Targeted polypharmacology: discovery of dual inhibitors of tyrosine and phosphoinositide kinases. *Nat. Chem. Biol.* **4,** 691–699 CrossRef Medline
18. Dar, A. C., Das, T. K., Shokat, K. M., and Cagan, R. L. (2012) Chemical genetic discovery of targets and anti-targets for cancer polypharmacology. *Nature* **486,** 80–84 CrossRef Medline
19. Wali, V. B., Langdon, C. G., Held, M. A., Platt, J. T., Patwardhan, G. A., Safonov, A., Aktas, B., Pusztai, L., Stern, D. F., and Hatzis, C. (2017) Systematic drug screening identifies tractable targeted combination therapies in triple-negative breast cancer. *Cancer Res.* **77,** 566–578 CrossRef Medline
20. Kangaspeska, S., Hultsch, S., Jaiswal, A., Edgren, H., Mpindi, J. P., Eldfors, S., Brück, O., Aittokallio, T., and Kallioniemi, O. (2016) Systematic drug screening reveals specific vulnerabilities and co-resistance patterns in endocrine-resistant breast cancer. *BMC Cancer* **16,** 378 CrossRef Medline
21. Sharma, S., and Petsalaki, E. (2018) Application of CRISPR-Cas9 based genome-wide screening approaches to study cellular signalling mechanisms. *Int. J. Mol. Sci.* **19,** E933 CrossRef Medline
22. Contreras, J. I., Robb, C. M., King, H. M., Baxter, J., Crawford, A. J., Kour, S., Kizhake, S., Sonawane, Y. A., Rana, S., Hollingsworth, M. A., Luo, X., and Natarajan, A. (2018) Chemical genetic screens identify kinase inhibitor combinations that target anti-apoptotic proteins for cancer therapy. *ACS Chem. Biol.* **13,** 1148–1152 CrossRef Medline
23. Wang, T., Birsoy, K., Hughes, N. W., Krupczak, K. M., Post, Y., Wei, J. J., Lander, E. S., and Sabatini, D. M. (2015) Identification and characterization of essential genes in the human genome. *Science* **350,** 1096–1101 CrossRef Medline
24. Tsherniak, A., Vazquez, F., Montgomery, P. G., Weir, B. A., Kryukov, G., Cowley, G. S., Gill, S., Harrington, W. F., Pantel, S., Krill-Burger, J. M., Meyers, R. M., Ali, L., Goodale, A., Lee, Y., Jiang, G., *et al.* (2017) Defining a cancer dependency map. *Cell* **170,** 564–576.e16 CrossRef Medline
25. Tan, L., Gurbani, D., Weisberg, E. L., Hunter, J. C., Li, L., Jones, D. S., Ficarro, S. B., Mowafy, S., Tam, C. P., Rao, S., Du, G., Griffin, J. D., Sorger, P. K., Marto, J. A., Westover, K. D., *et al.* (2017) Structure-guided development of covalent TAK1 inhibitors. *Bioorg. Med. Chem.* **25,** 838–846 CrossRef Medline
26. Tan, L., Gurbani, D., Weisberg, E. L., Jones, D. S., Rao, S., Singer, W. D., Bernard, F. M., Mowafy, S., Jenney, A., Du, G., Nonami, A., Griffin, J. D., Lauffenburger, D. A., Westover, K. D., Sorger, P. K., *et al.* (2017) Studies of TAK1-centered polypharmacology with novel covalent TAK1 inhibitors. *Bioorg. Med. Chem.* **25,** 1320–1328 CrossRef Medline
27. Hafner, M., Niepel, M., Chung, M., and Sorger, P. K. (2016) Growth rate inhibition metrics correct for confounders in measuring sensitivity to cancer drugs. *Nat. Methods* **13,** 521–527 CrossRef Medline
28. Hafner, M., Niepel, M., and Sorger, P. K. (2017) Alternative drug sensitivity metrics improve preclinical cancer pharmacogenomics. *Nat. Biotechnol.* **35,** 500–502 CrossRef Medline

29. Clark, N. A., Hafner, M., Kouril, M., Williams, E. H., Muhlich, J. L., Pilarczyk, M., Niepel, M., Sorger, P. K., and Medvedovic, M. (2017) GRcalculator: an online tool for calculating and mining dose-response data. *BMC Cancer* **17,** 698 CrossRef Medline
30. Russo, M., Di Nicolantonio, F., and Bardelli, A. (2014) Climbing RAS, the Everest of oncogenes. *Cancer Discov.* **4,** 19–21 CrossRef Medline
31. Stephen, A. G., Esposito, D., Bagni, R. K., and McCormick, F. (2014) Dragging ras back in the ring. *Cancer Cell* **25,** 272–281 CrossRef Medline
32. Lake, D., Corrêa, S. A., and Müller, J. (2016) Negative feedback regulation of the ERK1/2 MAPK pathway. *Cell. Mol. Life Sci.* **73,** 4397–4413 CrossRef Medline
33. Mendoza, M. C., Er, E. E., and Blenis, J. (2011) The Ras-ERK and PI3K-mTOR pathways: cross-talk and compensation. *Trends Biochem. Sci.* **36,** 320–328 CrossRef Medline
34. Chandarlapaty, S., Sawai, A., Scaltriti, M., Rodrik-Outmezguine, V., Grbovic-Huezo, O., Serra, V., Majumder, P. K., Baselga, J., and Rosen, N. (2011) AKT inhibition relieves feedback suppression of receptor tyrosine kinase expression and activity. *Cancer Cell* **19,** 58–71 CrossRef Medline
35. Rozengurt, E., Soares, H. P., and Sinnet-Smith, J. (2014) Suppression of feedback loops mediated by PI3K/mTOR induces multiple overactivation of compensatory pathways: an unintended consequence leading to drug resistance. *Mol. Cancer Ther.* **13,** 2477–2488 CrossRef Medline
36. Alexander, P. B., and Wang, X. F. (2015) Resistance to receptor tyrosine kinase inhibition in cancer: molecular mechanisms and therapeutic strategies. *Front. Med.* **9,** 134–138 CrossRef Medline
37. Lovly, C. M., and Shaw, A. T. (2014) Molecular pathways: resistance to kinase inhibitors and implications for therapeutic strategies. *Clin. Cancer Res.* **20,** 2249–2256 CrossRef Medline
38. Tolcher, A. W., Khan, K., Ong, M., Banerji, U., Papadimitrakopoulou, V., Gandara, D. R., Patnaik, A., Baird, R. D., Olmos, D., Garrett, C. R., Skolnik, J. M., Rubin, E. H., Smith, P. D., Huang, P., Learoyd, M., *et al.* (2015) Antitumor activity in RAS-driven tumors by blocking AKT and MEK. *Clin. Cancer Res.* **21,** 739–748 CrossRef Medline
39. Jiang, Z. B., Huang, J., Xie, C., Li, X., Liu, L., He, J., Pan, H., Huang, L., Fan, X. X., Yao, X. J., Xie, Y., Li, N., Liu, L., He, J. X., and Leung, E. L. (2016) Combined use of PI3K and MEK inhibitors synergistically inhibits lung cancer with EGFR and KRAS mutations. *Oncol. Rep.* **36,** 365–375 CrossRef Medline
40. Engelman, J. A., Chen, L., Tan, X., Crosby, K., Guimaraes, A. R., Upadhyay, R., Maira, M., McNamara, K., Perera, S. A., Song, Y., Chirieac, L. R., Kaur, R., Lightbown, A., Simendinger, J., Li, T., *et al.* (2008) Effective use of PI3K and MEK inhibitors to treat mutant Kras G12D and PIK3CA H1047R murine lung cancers. *Nat. Med.* **14,** 1351–1356 CrossRef Medline
41. Molina-Arcas, M., Hancock, D. C., Sheridan, C., Kumar, M. S., and Downward, J. (2013) Coordinate direct input of both KRAS and IGF1 receptor to activation of PI3 kinase in KRAS-mutant lung cancer. *Cancer Discov.* **3,** 548–563 CrossRef Medline
42. Suleymanova, N., Crudden, C., Worrall, C., Dricu, A., Girnita, A., and Girnita, L. (2017) Enhanced response of melanoma cells to MEK inhibitors following unbiased IGF-1R down-regulation. *Oncotarget* **8,** 82256–82267CrossRef Medline
43. Flanigan, S. A., Pitts, T. M., Newton, T. P., Kulikowski, G. N., Tan, A. C., McManus, M. C., Spreafico, A., Kachaeva, M. I., Selby, H. M., Tentler, J. J., Eckhardt, S. G., and Leong, S. (2013) Overcoming IGF1R/IR resistance through inhibition of MEK signaling in colorectal cancer models. *Clin. Cancer Res.* **19,** 6219–6229 CrossRef Medline
44. Wilky, B. A., Rudek, M. A., Ahmed, S., Laheru, D. A., Cosgrove, D., Donehower, R. C., Nelkin, B., Ball, D., Doyle, L. A., Chen, H., Ye, X., Bigley, G., Womack, C., and Azad, N. S. (2015) A phase I trial of vertical inhibition of IGF signalling using cixutumumab, an anti-IGF-1R antibody, and selumetinib, an MEK 1/2 inhibitor, in advanced solid tumours. *Br. J. Cancer* **112,** 24–31 CrossRef Medline
45. Rao, S., Gurbani, D., Du, G., Everley, R. A., Browne, C. M., Chaikuad, A., Li, T., Schröder, M., Gondi, S., Ficarro, S. B., Sim, T., Kim, N. D., Berberich, M., Knapp, S., Marto, J. A., *et al.* (2019) Leveraging compound promiscuity to identify targetable cysteines within the kinome. *Cell Chem. Biol.* CrossRef Medline

A multitargeted probe-based strategy to identify signaling vulnerabilities in cancers

Suman Rao, Guangyan Du, Marc Hafner, Kartik Subramanian, Peter K. Sorger and Nathanael S. Gray

J. Biol. Chem. 2019, 294:8664-8673.
doi: 10.1074/jbc.RA118.006805 originally published online March 11, 2019

SUPPLEMENTARY FIGURES AND TABLES

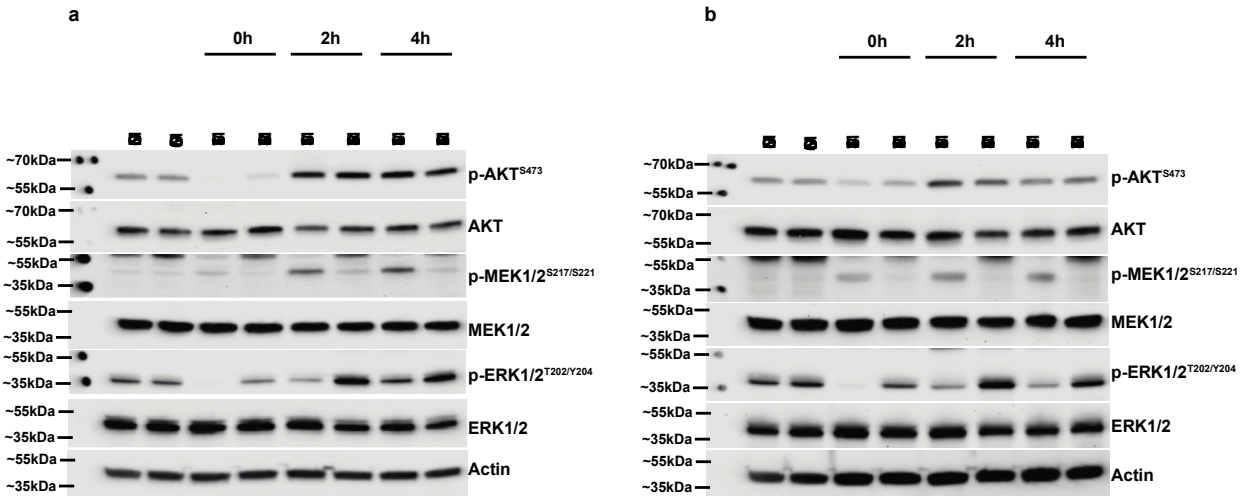

Figure S1: Two independent western blots demonstrating signaling effects in H23-KRAS^{G12C} cells upon treatment with SM1-71 or SM1-71-R, followed by washout (related to main figure 2a). Cells were treated with 1 μM SM1-71 or SM1-71-R (or DMSO) for 2h, followed by drug-washout and replacement with fresh media. Cells were extracted and lysed 0h, 2h and 4h post-washout and analyzed using western blotting. (**a)** and **(b)** represent blots from two independent experiments. Blot **a** has been shown in the main figure, 2a.

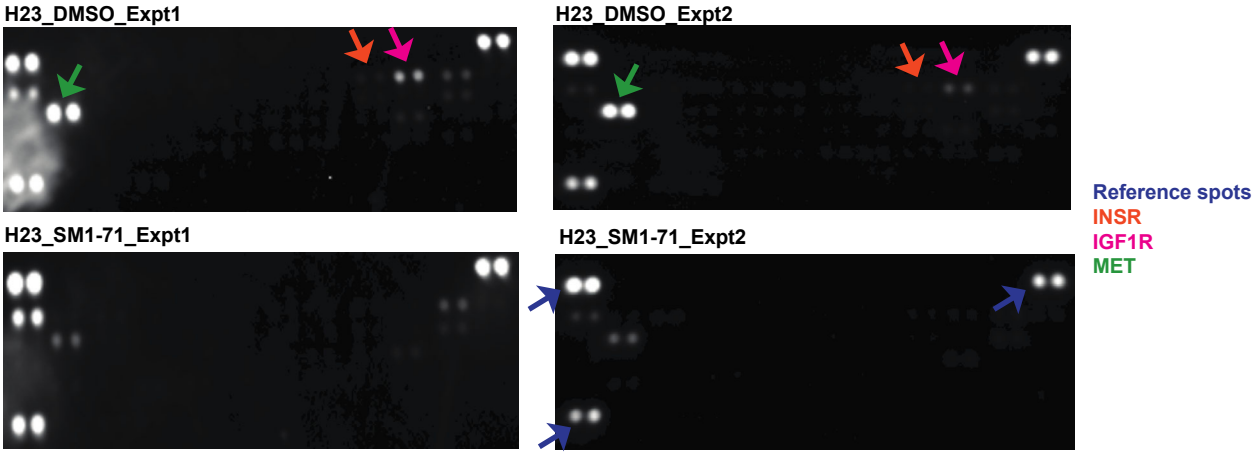

Figure S2: Phospho-RTK array blots measuring inhibition of RTKs upon treatment with SM1-71 (related to main figure 2b). Dot-blots illustrating phosphorylation states of RTKs derived from H23-KRAS^{G12C} cells treated with DMSO or SM1-71 (1 μM) for 6h. Upon treatment, cells were collected, lysed and incubated with the array blots, followed by brief incubation with a secondary HRP-conjugated phospho-tyrosine antibody and signal readout using chemiluminescence. Quantification of blots was carried out using the dot-blot analyzer (imageJ), which are represented as bar-graphs in Fig. 2b.

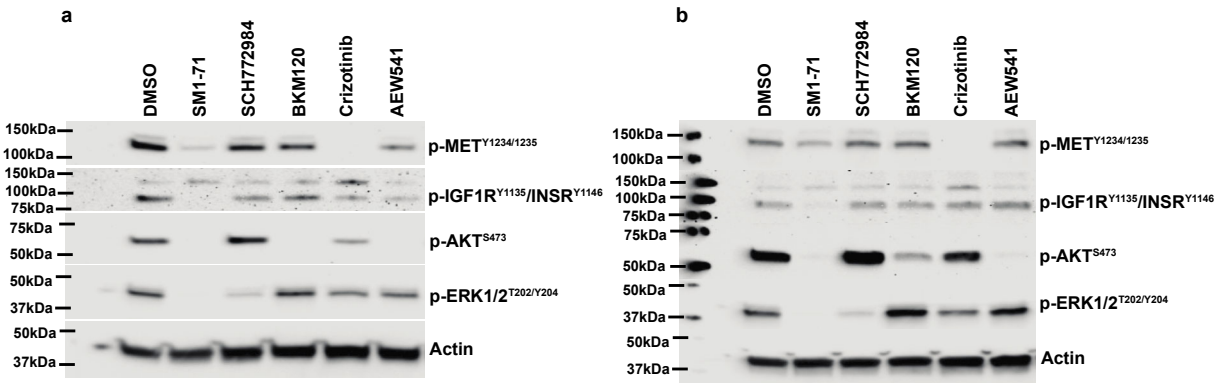

Figure S3: Two independent western blots demonstrating signaling effects downstream of IGF1R and MET in H23-KRAS^{G12C} cells (related to main figure 2c). Cells were treated with 1 μM SM1-71, SCH772984 (ERK), BKM120 (PI3K), crizotinib (MET), AEW541 (IGF1R) or DMSO for 4h, followed by extraction and lysis. Phosphorylation of MET, IGF1R/INSR, AKT and ERK1/2 was detected using antibodies in a Western blot assay. Blots from both experiments are represented in **(a)** and **(b)** and blot **b** is shown in the main figure 2c.

Table S1: List of kinases inhibited by SM1-71 (>1.5-fold) and their corresponding IC_{50} values, as determined by a Multiplexed Inhibitor Beads (MIB) assay (Rao et al, Cell Chem Biol, accepted, 2019)

Kinase	IC50 (nM)
GAK	0.8
YES1	0.8
SRC	2
AAK1	4.4
LIMK1	5.4
BMP2K	7.1
MAP2K2	9.3
AURKA	10.3
MAP2K1	10.4
MAP3K1	28.7
TEC	31.8
PTK2	36.4
MAPK1	48.3
MAPK3	107
MARK2	135.5
WEE1	145
PRKD3	166
LYN	187
TGFBR2	577

IGF1R	600
INSR	767
TNIK	6919
DDR1	8400
MET	10000
CSNK2A1	>10000
EPHA10	>10000
CSNK1E	>10000
EPHB2	>10000
EPHA2	>10000
PIP4K2C	>10000
AGK	>10000
PKMYT1	>10000
CDK9	>10000
STK16	>10000
PIP5K1A	>10000
CDK13	>10000
CSNK1G1	>10000
CDK17	>10000
MAP3K11	>10000
TGFBR1	>10000
ACVR1B	>10000
TK2	>10000
PRKDC	>10000
CSNK1A1	>10000
CSNK1D	>10000
CSNK1G3	>10000
PAK4	>10000
FGFR1	/
PIK3C3	/
PIK3R4	/
ACVR1	/
EIF2AK3	/
HCK	/
FYN	/

Table S2: Average GR_{50} (μM), GR_{max} and R^2 values from two independent growth inhibition assays across a panel of cancer cell lines

treatment	cell_line	GR50	GRmax	r2_GR
SM1-71	A375	0.07	-0.49	0.92
SM1-71	H1975	0.04	-0.67	0.99
SM1-71	H23	0.06	-0.67	0.99
SM1-71	H3122	0.25	-0.44	0.95
SM1-71	H460	1.22	0.26	0.88
SM1-71	HCC827	0.07	-0.61	0.93
SM1-71	HCT116	0.07	-0.33	0.98
SM1-71	MDAMB231	0.02	-0.87	0.98
SM1-71	MDAMB453	1.50	-0.57	0.93
SM1-71	MDAMB468	0.01	-0.79	0.86
SM1-71	MiaPaca2	0.08	-0.41	0.82
SM1-71-R	A375	0.29	0.01	0.55
SM1-71-R	H1975	0.36	-0.60	0.97
SM1-71-R	H23	0.38	-0.34	0.97
SM1-71-R	H3122	0.28	-0.37	0.96
SM1-71-R	H460	2.33	0.25	0.93
SM1-71-R	HCC827	0.35	-0.60	0.97
SM1-71-R	HCT116	0.74	-0.06	0.76
SM1-71-R	MDAMB231	0.16	-0.71	0.98
SM1-71-R	MDAMB453	3.59	0.07	0.80
SM1-71-R	MDAMB468	0.01	-0.68	0.89
SM1-71-R	MiaPaca2	0.17	-0.40	0.86
AZD6244	A375	0.79	0.48	0.90
AZD6244	H1975	37.7*	0.69	0.81
AZD6244	H23	2.47	0.40	0.90
AZD6244	H3122	3.76	0.28	0.92
AZD6244	H460	1619*	0.87	0.51
AZD6244	HCC827	149.00	0.81	0.44
AZD6244	HCT116	17.30	0.56	0.86
AZD6244	MDAMB231	1.24	0.21	0.93
AZD6244	MDAMB453	Inf*	0.90	0.10
AZD6244	MDAMB468	171*	0.74	0.22
AZD6244	MiaPaca2	5.15	0.46	0.74
BKM120	A375	1.75	0.22	0.92
BKM120	H1975	0.76	-0.19	0.99
BKM120	H23	0.93	-0.51	0.97
BKM120	H3122	1.23	-0.37	0.96
BKM120	H460	2.33	0.32	0.97
BKM120	HCC827	1.43	-0.15	0.96

BKM120	HCT116	1.74	0.02	0.96
BKM120	MDAMB231	1.21	-0.13	0.98
BKM120	MDAMB453	0.65	-0.57	0.99
BKM120	MDAMB468	1.12	-0.32	0.96
BKM120	MiaPaca2	1.03	0.27	0.80
Ceritinib	A375	2.94	-0.47	0.95
Ceritinib	H1975	2.67	-0.75	0.98
Ceritinib	H23	1.76	-0.88	0.94
Ceritinib	H3122	0.05	-0.78	0.96
Ceritinib	H460	4.37	-0.51	0.89
Ceritinib	HCC827	3.53	-0.73	0.85
Ceritinib	HCT116	2.97	-0.50	0.99
Ceritinib	MDAMB231	2.73	-0.91	0.98
Ceritinib	MDAMB453	2.48	-0.87	0.98
Ceritinib	MDAMB468	2.60	-0.82	0.97
Ceritinib	MiaPaca2	2.92	-0.78	0.83
Lapatinib	A375	17.7*	0.83	0.57
Lapatinib	H1975	69.2*	0.75	0.64
Lapatinib	H23	9.76	0.45	0.82
Lapatinib	H3122	10.5*	0.55	0.72
Lapatinib	H460	116*	0.88	0.28
Lapatinib	HCC827	1.27	-0.47	0.96
Lapatinib	HCT116	79.4*	0.72	0.57
Lapatinib	MDAMB231	6.87	0.13	0.94
Lapatinib	MDAMB453	2.20	-0.28	0.84
Lapatinib	MDAMB468	2.69	-0.14	0.80
Lapatinib	MiaPaca2	62.8*	0.61	0.48
Osimertinib	A375	4.51	-0.42	0.90
Osimertinib	H1975	0.20*	-0.70	0.64
Osimertinib	H23	4.88	-0.45	0.98
Osimertinib	H3122	2.00	-0.71	0.99
Osimertinib	H460	9.61	0.48	0.81
Osimertinib	HCC827	0.03*	-0.63	0.69
Osimertinib	HCT116	4.95	-0.45	0.99
Osimertinib	MDAMB231	3.29	-0.89	0.98
Osimertinib	MDAMB453	1.85	-0.85	0.90
Osimertinib	MDAMB468	1.42	-0.80	0.90
Osimertinib	MiaPaca2	4.83	-0.65	0.92
SCH772984	A375	Inf	0.52	0.67
SCH772984	H1975	17.3	0.60	0.90

SCH772984	H23	0.53	0.21	0.96
SCH772984	H3122	0.22	-0.16	0.98
SCH772984	H460	53.4*	0.78	0.77
SCH772984	HCC827	30.1*	0.65	0.56
SCH772984	HCT116	0.43	0.18	0.93
SCH772984	MDAMB231	0.15	0.18	0.97
SCH772984	MDAMB453	59.2*	0.67	0.60
SCH772984	MDAMB468	4.03	0.37	0.49
SCH772984	MiaPaca2	0.30	0.30	0.76
Vemurafenib	A375	1.13	0.43	0.91
Vemurafenib	H1975	43.7*	0.76	0.82
Vemurafenib	H23	Inf*	0.92	-0.38
Vemurafenib	H3122	Inf*	0.90	0.47
Vemurafenib	H460	112*	0.90	0.37
Vemurafenib	HCC827	Inf*	0.81	0.35
Vemurafenib	HCT116	103*	0.87	0.64
Vemurafenib	MDAMB231	Inf*	0.94	0.05
Vemurafenib	MDAMB453	42.3*	0.89	0.18
Vemurafenib	MDAMB468	Inf*	0.93	0.01
Vemurafenib	MiaPaca2	Inf*	1.01	-0.67

*The exact GR_{50} values for these compounds are unclear due to poor curve-fit ($R^2 < 0.8$).

Notes:

1: Cells were treated 24h following plating and maintained in the presence of compounds for a period of 72h.

2: All calculations have been generated using the GR Calculator (http://www.grcalculator.org/grcalculator_dev/). These values represent the average from two independent experiments, each dose treated in technical triplicate. To view all fitted parameters from the analysis, please refer to supplemental file 1.